# Intermediate-mass black hole binary merger as the origin of supermassive black holes

*Isabelle Thord*

Division of Astrophysics
Department of Physics
Lund University

2023-EXA205

Degree project of 15 higher education credits
June 2023

Supervisor: Ross Church

Division of Astrophysics
Department of Physics
Box 43
SE-221 00 Lund
Sweden

**Abstract**

Galactic nuclei contain super-massive black holes (SMBHs), nuclear stellar clusters (NSCs), or both. In the NSC, intermediate-mass black holes (IMBHs) are likely to reside and form highly eccentric binaries. Over time, the orbit of a binary could harden via interaction with surrounding low-mass stars. Eventually, it would be possible for the IMBHs to, via the emission of gravitational waves (GWs), merge into an SMBH seed that over time can grow and result in an SMBH in the galactic nuclei.

The aim of this thesis is to establish under what circumstances mergers occur. I wish to track which encounters are most responsible for taking the binary from formation to merger and see if this can happen within a reasonable astrophysical merger time. This would shine a light on whether IMBH binary mergers are possible and, by extension, further motivate the attempted detections of GWs from these events. Moreover, it would reinforce IMBH binaries as a possible origin of SMBH seeds in the NSC. I aim to also investigate the importance of different parameters such as mass ratio and initial eccentricity to see what part they play in bringing the system to a point of merger.

Multiple N-body simulations of an IMBH binary and a lower mass impactor were carried out via the TSUNAMI code. Its output was then utilized when tracking the evolution of the semi-major axis and eccentricity and how different encounters affected the binary. Besides that, the output was used when investigating the effect of altering previously mentioned parameters. The evolution of the system was put in relation to a Toy model and N-body run presented by Askar et al. (2021). Despite the simulations' stochastic nature, it was found that the investigated IMBH binary significantly hardened during an encounter-driven evolution whilst staying noticeably eccentric. This allowed the binary to reduce its astrophysical merger time which enabled SMBH seed formation. But whilst this all qualitatively aligns with the findings of Askar et al. (2021), it was established that the assumptions embedded in the Toy model led it to exhibit an unrealistic eccentricity pumping. What mainly separated the here performed simulations from those in the Toy model was the assumption that each encounter affected the whole binary instead of only one constituent, as was the case in the Toy model.

It was discussed how there was no obvious change in merger time from an altered initial eccentricity but how a lower impacting mass was less efficient in bringing the system to a merger. When allowing for wider encounters the results were somewhat ambiguous and require more investigation before any conclusions can be drawn. Each simulated encounter had a unique offset, velocity, and encounter time but to further elaborate on the finding of this thesis, assumptions such as the third mass being constant and the body's point-like behaviour should be re-evaluated.

## Populärvetenskaplig beskrivning

Att påverkas av andra är något för oss så naturligt att vi sällan tänker på hur ofta det händer. En annan kropps närvaro kan ge oss energi lika väl som ta den ifrån oss. Den kan få oss att vilja komma närmare eller längre ifrån. Detta samspel är inte unikt för oss människor, utan kan även ses på himlavalvet. På universums dansgolv finner vi par av alla dess slag. Särskilt mystiska är kanske de svarta hål som valt att dansa kring varandra på sin resa genom havet av åskådare. Bland gästerna finner vi stjärnor som, precis som balgäster, kommer närma sig för att interagera med paret. Dessa möten kommer påverka vår duo som antingen drar sig lite närmare varandra eller ökar avståndet mellan sig, beroende på om stjärnans närvaro tar eller ger energi.

Nyligen presenterades en teori om att ett par bestående av svarta hål på ett tätt packat dansgolv bör bli så påverkat av alla möten att de väljer att slå sig sammantill ett massivt svart hål. Inte bara det, utan att desto fler möten som är dränerande, desto mer benägna blir de att gå samman. Min fråga är: vilka möten påverkar paret mest och hur länge behöver de utstå dränerande möten innan de bestämmer sig för att bli ett? Genom att simulara två svarta håls dans kring varandra i ett hav av närgångna stjärnor kom jag fram till att de mest påträngande tredje parterna drev paret närmare varandra och att den model som tidigare presenterats kanske inte berättade hela historien. Men att de två svarta hålen gick samman och bildade ett stort svart hål, det var det ingen tvekan om.

# Contents

# Chapter 1

# Introduction

At the center of most galaxies, there is a massive stellar cluster of high density, referred to as a nuclear star cluster (NSC: Neumayer et al. 2020). This has been found to be formed in situ (Loose et al. 1982; Aharon & Perets 2015) or through a cluster-/infall scenario (Mastrobuono-Battisti et al. 2014). Antonini et al. (2012) found that in the Milky Way, the NSC is likely to originate in equal amounts from in situ formation as from merging stellar clusters.

In the cluster-/infall scenario, it has been established that merging stellar clusters generally migrate toward the galactic center as a result of dynamical friction (Tremaine et al. 1975; Tsatsi et al. 2017) and thereby form the NSC. The formation might include infalling clusters that are hosting intermediate-mass black holes (IMBHs) of masses $10^2 - 10^4 M_\odot$ (Mastrobuono-Battisti et al. 2014), which are brought into the NSC (Ebisuzaki et al. 2001; Mastrobuono-Battisti et al. 2014).

Through numerical simulations, it has been shown how IMBHs could stem from massive stars (Gürkan et al. 2004; Portegies Zwart et al. 2004, 2006; Freitag et al. 2006; Fujii et al. 2009). These stars would be generated via runaway collisions between smaller stars and then, due to dynamical friction, sank to the bottom of the potential well located in the center of the cluster and collapsed into IMBHs. IMBHs could also be the result of a smaller-sized black hole that has accreted gas over a long time (Leigh et al. 2013). A third option of IMBH formation is a Population III star that has collapsed (Madau & Rees 2001)

The recurring formation of binaries in stellar clusters was established by Heggie (1975a). Larson (1970a,b), Hénon (1972a,b) and Spitzer & Hart (1971a,b) had previously investigated how neglecting binary formation affected the simulation of cluster evolution. They found that more and more energy was still being shared by fewer members of the core whilst its overall mass decreased. The arising of energetic

binaries was thereby inevitable in the evolution of a cluster (Heggie 1975a). One application of this is when multiple IMBHs are brought into the NSC (Mastrobuono-Battisti et al. 2014). An IMBH-binary is two IMBHs that orbit each other due to their respective gravitational pull. Most IMBH binaries form at moderate to high eccentricities (Askar et al. 2021).

Binaries can merge by emitting gravitational waves (GWs: Amaro-Seoane & Freitag 2006; Wirth & Bekki 2020). What is clear from the already existing research, such as Askar et al. (2021), is that merged IMBHs can serve as a super-massive black hole (SMBH) "seed". The recoil kick from the GWs, emitted during the merger, in relation to the escape speed of the galactic nucleus, determines whether or not the seed can remain within the NSC. If it does, it can grow into an SMBH by accreting surrounding stars (Amaro-Seoane & Freitag 2006; Wirth & Bekki 2020). However, if the recoil kick exceeds the escape speed of the NSC, the seed will be ejected from the galactic nucleus (Askar et al. 2021).

However, IMBH merger is not the only possible origin of SMBH seeds. Another possible explanation is the collapse of a giant star. The collapse could result in a black hole seed with an initial mass of the order $10^5$ $M_\odot$ that then would grow by accretion (Volonteri 2010; Greene et al. 2020).

For an IMBH binary to merge, its orbit must be sufficiently narrow and eccentric. For simultaneous values of eccentricity $e$ and semi-major axis $a$, Peters (1964) present a corresponding merger time

$$\tau_{\rm gr} \simeq 10^{10}_{\rm yr} \left( \frac{a_{\rm bin}}{3.3 R_\odot} \right)^4 \frac{1}{(m_1 + m_2) m_1 m_2} (1 - e^2)^{7/2} \tag{1.1}$$

where $e$ is the eccentricity and $m_1$ and $m_2$ are the masses of the binary constituents. When the merger time in Eq 1.1 is less than the average time between encounters, a merger is expected to occur. The average time between encounters is given by Askar et al. (2021) as

$$\Delta t_{enc} = \frac{1}{n \sigma \pi b_{max}^2} \tag{1.2}$$

where $n$ is the number density of the NSC, $\sigma$ is the velocity distribution given in Table 2.1 and $b_{max}$ is the maximal impact parameter of the third body.

The relevant IMBH binaries from merging clusters are according to Askar et al. (2021) formed with a semi-major axis of about 4000 a.u. What then drives the semi-major axis to lower values, and via Eq 1.1 also shorter merger times, is encounters with surrounding stars (Begelman et al. 1980). Since this thesis focuses on binaries in the NSC, the stars will also lie in this region of the galaxy.

## 1.1 Hardening

If the initial binding energy of a binary exceeds the average binding energy of stars in the clusters, it is considered hard (Dokuchaev & Ozernoi 1981). If a hard binary has a wide encounter with a third body, it will typically lose kinetic energy to the passerby (Begelman et al. 1980). This leds to a change in both binding energy and eccentricity. If the semi-major axis shrinks, it is classified as a *hardening* of the binary (Begelman et al. 1980). Hardening will proceed until the point of GW-generated merger if the stars in the loss cone are not all ejected. The loss-cone is a region of orbits that pass sufficiently close to be gravitationally affected by the binary and potentially get ejected from the NSC by interaction with the binary (Magorrian & Tremaine 1999). If all stars in the loss cone are ejected, the binary should simply survive the lifetime of its host galaxy. I will assume that the loss cone is constantly refilled via dynamical processes. These include interactions between stars that cause their orbits to diffuse into the loss cone.

A previous study on IMBH binary mergers in the NSC was carried out by Askar et al. (2021). They performed an N-body run (see Run 2.2 in Askar et al. (2021)) as well as proposed a toy model (here referred to as the Toy model) of IMBH mergers as a result of multiple encounters. An optimal encounter would generate an increase in the eccentricity accompanied by a decrease in the semi-major axis (Heggie 1975a) until the orbit was sufficiently narrow for the binary members to be close enough to merge. If an encounter occurred at the pericentre or apocenter, the eccentricity of the orbit would decrease or increase respectively. Statistically, more encounters between an IMBH binary and low-mass stars should arise whilst the binary is at apocentre due to a larger part of the period being spent there (Askar et al. 2021). Over time, this means that the binary should harden and go towards a more eccentric orbit, eventually resulting in a merger. It is this evolution of the binary's orbit that I want to expand via a Monte Carlo approach.

# Chapter 2

# Method

## 2.1 Stochastic orbital evolution

For every interaction, I intend to track changes in the binary's semi-major axis and eccentricity as previously done by Askar et al. (2021). Not only do I aim towards recreating the setup of the Toy model presented by Askar et al. (2021) but I wish to investigate the characteristics of the encounters in a more rigorous manner. From the presentation of the Toy model, it is not clear which encounters are mainly responsible for the binary's evolution or what encounters are included. I also intend to compare my simulations with respect to the N-body run executed by Askar et al. (2021), so as to weed out which of the assumptions done by the models can be reinforced and dismissed. On the spectrum of completeness and complexity, the Toy model and N-body run are on opposite sides whereas I aim for the middle.

### 2.1.1 Dynamics of the system

#### Initial set up

The system in the Toy model from Askar et al. (2021) is an IMBH binary and a third body, here a low-mass star from the surrounding NSC. This is illustrated in Figure 2.1 and the related parameters are displayed in Table 2.1. At infinite separation, the third body has an approach velocity of $\vec{v_\infty}$. I assume the masses in the system to remain constant since the bodies in the model by Askar et al. (2021) never collide.

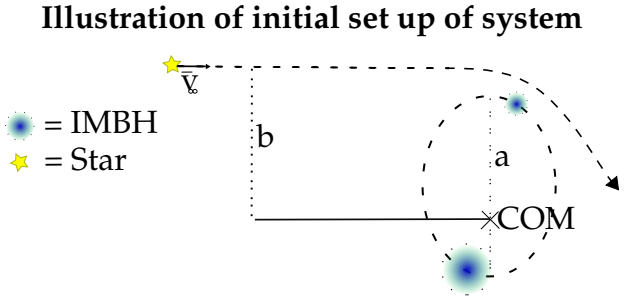


**Figure 2.1:** Initial set up of a three-body system where the third body is represented by a star. the third body's offset from the binary's center-of-mass in denoted $b$ and at infinite separation, the third body has velocity $\vec{v_\infty}$. The binary consists of two IMBHs in an orbit with a semi-major axis $a$. Note, the figure is not to scale and should be viewed as an illustration and not a physical representation.

**Table 2.1:** Properties of system in Toy model from paper by Askar et al. (2021).

| Parameter | value |
|---|---|
| $M_1$ | $10^3$ $M_\odot$ |
| $M_2$ | $10^2$ $M_\odot$ |
| $M_3$ | 1 $M_\odot$ |
| $\sigma$ | 15 $\frac{km}{s}$ |
| $e_0$ | 0.996 |
| $a_0$ | 4000 a.u |

### Distribution of impact parameter $b$

With the assumption that the closer an encounter is to the binary's center of mass (COM) the more impact it has on the pair, comes the limit of the separation where the encounter will no longer have an effect. The smallest distance to the COM along the third body's trajectory $r_{\text{peri}}$ should therefore be proportional to the size of the binary, i.e

$$r_{\text{peri}} \propto a(1+e). \tag{2.1}$$

From energy and angular momentum conservation, the third body's maximum separation from the COM's axis parallel to the initial velocity $v_\infty$, marking the line be-

tween impactful and unimpactful encounters, becomes

$$b_{\max} = r_{\text{peri}}\sqrt{1+\frac{2M_T}{r_{\text{peri}}v_\infty^2}} = Ca(1+e)\sqrt{1+\frac{2M_T}{Ca(1+e)v_\infty^2}}. \tag{2.2}$$

Here, $M_T$ is the total mass of the system and $C$ a proportionality constant.

Each encountering third body's displacement $b$ (see Figure 2.1) will be randomly located in a probability distribution ranging from zero to $b_{max}$. Given a ring that is concentric with the binary's COM and has a thickness db<$b_{max}$, the area of the inner circle is lesser than that between db and $b_{max}$. Accounting for this when generating the a $b$ practically becomes expressing the probability that $b$ is smaller than a some value $b_i$, i.e utilising the cumulative distribution function. This entails the probability of $b$ being smaller than a $b_i$, $P(b < b_i)$, being proportional to the area $\pi b_i^2$ as well as being equal to one when $b_i = b_{max}$. This can be mathematically expressed as

$$P(b < b_i) = \frac{\pi b_i^2}{\pi b_{\max}^2} = \frac{b_i^2}{b_{\max}^2} = x$$

where $x$ ranges from 0 to 1. This probability is utilised as the random factor for the location of the impact parameter $b$.

Through Eq 2.2, the change in the semi-major axis was investigated, via plotting, as a function of impact parameter $b$. This was done for a range of $v_\infty$. One of these plots is displayed in Figure 2.2. Based on these plots, the condition of a relevant encounter was deemed to be one that causes a change in $a$ of order $10^{-5}$ or greater. Such a low limit was considered to be enough to include all encounters causing a noticeable change in $a$, as displayed in Figure 2.2.

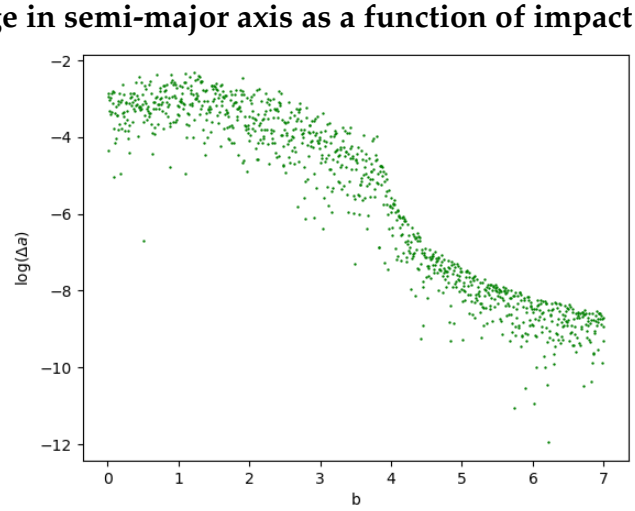


**Figure 2.2:** Change in semi-major axis $a$, whose initial value is presented in Table 2.1, as a function of impact parameter $b$. It can be noted that the envelope of the distribution ends somewhere around $log(\Delta a) = -5$ which was where the limit of relevant encounters was set.

As can be observed in Eq 2.2, the constant $C$ has a dependence on $\vec{v_\infty}$ and dictates the outcome of $b_{\max}$. Therefore, $C$ was plotted as a function of values of $v_\infty$. Once its maximum had been located, at a value of C=6.116, it was put as this constant value. This enabled $b$ to be randomly chosen, via $x$, within a set range, dictated by $C$ through Eq 2.2.

**Choice of $v_\infty$**

Along with $b$, $v_\infty$ should be unique for each encountering star to maintain a realistic setup of the simulation. The value of each $v_\infty$ was generated by letting each dimensional parameter be taken from a Gaussian distribution of width $\sigma$. Here, $\sigma$ is the standard deviation and has a set value of 15 km/s, see Table 2.1, in accordance with Askar et al. (2021). This procedure generated a distribution of $v_\infty$ that followed a form of the Maxwell-Boltzmann distribution (Ryden & Peterson 2021a, eq. 5.40)

$$f(v_\infty, \sigma) = \frac{4\pi}{(2\pi)^{3/2}} v_\infty^2 e^{-v_\infty^2/2\sigma^2}. \tag{2.3}$$

### 2.1.2 TSUNAMI - evolution of system

TSUNAMI is a C++ code evolving three (or few) body systems over time (Trani & Spera 2020). It aims to optimize accuracy as well as avoid numerical and time-related issues when the bodies in the system get closer.

Due to TSUNAMI's implementation of a modified solution to the Newtonian equations of motion (Mikkola & Tanikawa 1999a,b), a property of the code is its fictitious time step not being equal to its physical counterpart. This allows the user to follow the evolution of the system even as bodies get close and forces diverge. Since my interest lies in tracking the details of encounters, this property of TSUNAMI is crucial.

I chose to let TSUNAMI's running time be based on physical restraints instead of a set finishing time. This is because the length of encounters was not equal but instead depended on how hard the binary was as well as the approach velocity of the third body. The physical conditions, allowing TSUNAMI to evolve the system in time, were therefore given to be that the third body had to be within a distance such that it was affected by the binary or it had to be approaching the binary. The distance of relevance was set to 20 times $a$ or $b$, whichever was the largest. This ensured the simulation accounted for distances where the bodies affected each other as well as a margin.

This combination of constraints allowed the system to have a dynamic evolution within the encounter. This is physically relevant to include, to increase the level of reliability. However, it was of interest to detect whether the dynamical evolution was short- or long-termed. To do this, the encounter time was compared to the time of a straightforward encounter $2\frac{D}{v_\infty}$ where $D$ is the distance between the third body and the binary's center of mass (Heggie 1975b). The ratio was used to indicate any anomalies, such as the short-term dynamical evolution displayed in Figure 2.3. Here is an example of transient triple formation, meaning the third body does one or more laps around the binary before being ejected out of orbit (Valtonen & Karttunen 2006; Heggie 1975b).

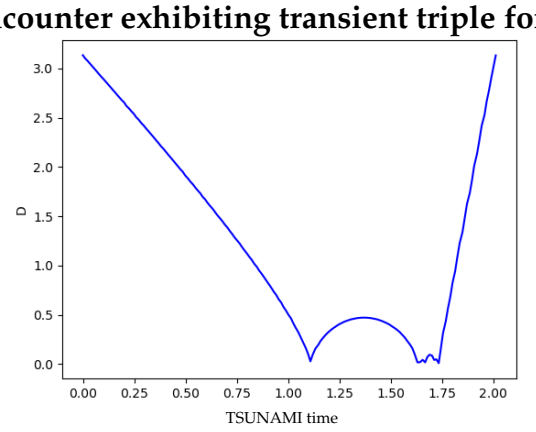


**Figure 2.3:** Plot illustrating the third body's distance $D$ to the binary's center-of-mass as a function of the time it takes TSUNAMI to simulate the encounter. It shows a clear example of hardening, as is indicated by one side being steeper than the other. This corresponds to the third body exiting with a higher velocity than it approached with. The clear bumps are caused by transient triplet formation where the third body gives energy to - instead of receives energy from - the binary and therefore falls into orbit for a short period of time (Valtonen & Karttunen 2006; Heggie 1975b).

Besides the case shown in Figure 2.3, there was still the statistical probability of the third body getting gravitationally bound into a seemingly endless orbit. This occurred when the third body gave, instead of received, energy and became bound in a low-energy orbit around the binary. Such orbits can have close to infinite periods and have a statistical risk of occurring (Valtonen & Karttunen 2006; Heggie 1975b). These infinite orbits were neglected by setting an upper boundary to the run time of $\frac{10D}{v_\infty}$.

Within the TSUNAMI code, the user can choose their own units. The chosen units of the TSUNAMI code are displayed in Table 2.2 and were taken from Askar et al. (2021).

**Table 2.2:** Units of relevant parameters as given by Askar et al. (2021).

| **Parameter** | **Unit** |
|---|---|
| Mass | $10^3$ $M_\odot$ |
| Length | 4000 AU |
| G | 1 |
| Velocity | 14.8 km/s |

### 2.1.3 Simulations

#### Necessary mathematics

The binary's kinetic energy $T$ and potential energy $V$ depend on the velocity $\vec{v}$ and position $x$ of the elements and sums to the binary's total energy. In its turn, the total energy $E_{1,2}$ of the binary has a dependence on the semi-major axis $a$, allowing for its extraction once $E_{1,2}$ is established,

$$E_{1,2} = T_{1,2} + V_{1,2} = \frac{1}{2}\mu|\vec{v_1} - \vec{v_2}|^2 - \frac{Gm_1m_2}{|\vec{x_1} - \vec{x_2}|} = -\frac{Gm_1m_2}{2a}. \tag{2.4}$$

Here, $\mu$ is the reduced mass of the binary, i.e $\mu = \frac{m_1m_2}{m_1+m_2}$.

Similarly, the angular momentum $j$ has a dependence on the eccentricity $e$ on the shape of

$$\left|\vec{j}\right| = |(\vec{x_1} - \vec{x_2}) \times (\vec{v_1} - \vec{v_2})| = \sqrt{GMa(1-e^2)} \tag{2.5}$$

where $G$ is the gravitational constant and $M$ is the sum of the binary element's masses (Valtonen & Karttunen 2006). The eccentricity is defined as the difference between apoapsis and periapsis over the apsoline (Ryden & Peterson 2021b). A circular orbit means $e = 0$ whilst an elliptical orbit has $0 < e < 1$.

#### Execution

All computational parts are done in Python except for TSUNAMI, which runs in C++ but has a Python envelope that has been used to run it.

A function taking the parameters marked out in Figure 2.1 and the masses from Table 2.1 was constructed by Ross P. Church. This took a semi-major axis, eccentricity, impact parameter, and $v_\infty$ as input and gave the initial positions and velocities of the system as an output. Due to $v_\infty$ and $b$ being unique for each encounter, the simulations were non-deterministic. A random seed was therefore implemented to allow for repeatable results (Kaczmarczyk & Miałkowska 2022).

I evaluated these vectors in time using TSUNAMI's three-body scattering program (see Section 2.1.2). For each instance in time, the position and velocity of each body were tracked. I used these vectors to acquire $a$ and $e$ for every point in time via Eq 2.4 and 2.5 as well as $b$ and $v_\infty$ for each encountering body. The outputs allowed me to see how the encounter affected the binary and if the initial masses and separations generated a hardening, softening, or no interaction whatsoever. The conditions for what was considered an encounter are described in Section 2.1.1.

# Chapter 3

# Results

## 3.1 Stochastic orbital evolution

Evaluating a binary with masses $10^3$ $M_\odot$ and $10^2$ $M_\odot$ that repeatedly have encounters with an impactor of mass 1 $M_\odot$ resulted in noticeable hardening of the binary as it evolves from right (log(a)$\approx$ 3.5) to left (log(a)$\approx -1$) in Figure 3.1. The impactor has an initial velocity $v_\infty$ and an impact parameter $b$ whose determinations are described in Sections 2.1.1. The initial conditions were taken from Askar et al. (2021) and entailed a semi-major axis $a$ of 4000 a.u and an eccentricity of $e$=0.996. In the aim to replicate the length of the evolution in Askar et al. (2021), the simulations stopped when the semi-major axis had shrunk to $4 \cdot 10^{-2}$ a.u.

Along with the solid line which is representative of the state of the binary, merger time contours are displayed in Figure 3.1. These are derived from Eq 1.1 and are indicators of how long it would take a binary with a specific set of $a$ and $e$ to merge via GW emission if the rate of encounters would stagnate. For the binary to merge in between encounters, the current merger time has to be shorter than the average time between encounters.

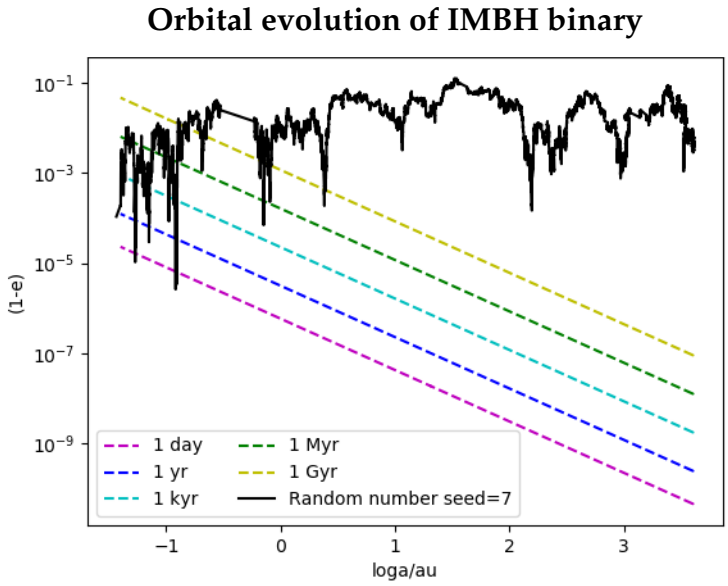


**Figure 3.1:** One minus eccentricity over semi-major axis. The solid line represents the evolution of an IMBH binary that hardens via encounters with $3.8 \cdot 10^3$ surrounding low mass stars. Displayed are also diagonal merger times contours derived from Eq 1.1. As observable, hardening allows the system to reach parameters allowing for a merger within a day at about log(a)=-0.9.

The orbital evolution, in Figure 3.1, exhibits the expected hardening as suggested by Askar et al. (2021). The eccentricity stays high, as indicated by *1-e* going down to below $10^{-5}$, and fluctuates continuously throughout the evolution of the system. The fluctuations can be explained by the evolution being stochastic whilst the hardening and lack of eccentricity lowering confirms the hardening phenomena described in Section 1.1 and by Askar et al. (2021). During its evolution, the binary reaches considerably short merger times. This indicates that encounters with low-mass stars are an efficient way for an IMBH binary to merge into a SMBH seed.

### 3.1.1 Which encounters matter?

Normalized histograms of the number density of encounters causing corresponding changes in $a$ and $e$ are displayed in Figure 3.2a and 3.2b, respectively. For the positive and negative changes in $a$, the ratios were 49.6% and 50.4% respectively. Similarly, the ratios for positive and negative changes in $e$ were 49.8% and 50.2%. This aligns well with the evolution being stochastic and there being a slight energetic preference towards hardening.

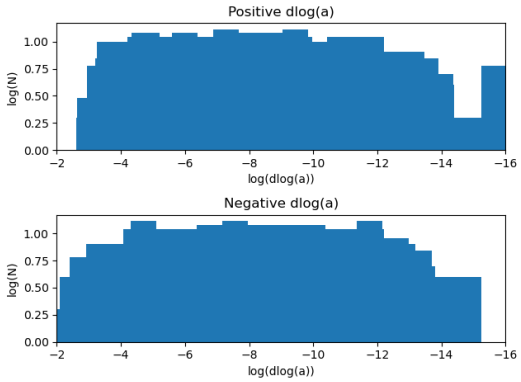


**(a)** Normalised histogram of changes in the semi-major axis. Note how the distribution is flat in shape. This indicates there not being an over-representation of any kind of encounter. Thereby, the most impactful encounters are those driving the evolution of the binary.

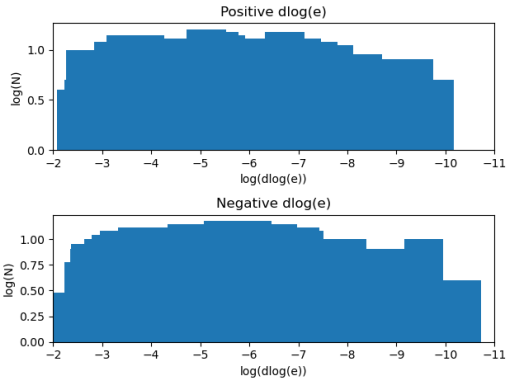


**(b)** Normalised histogram of changes in eccentricity. The same trend is seen here as in Figure 3.2a and the same conclusion can therefore be drawn. Similarly to Figure 3.2a the plateau starts at -3 and these should therefore be the most dominant encounters in the evolution.

**Figure 3.2:** Histograms over changes in semi-major axis and eccentricity. They agree and display that strong encounters dictate the evolution of the binary.

Both the histograms of changes in $a$ and $e$ exhibit plateau-like shapes starting at -3. There not being any obvious peaks indicates that the encounters mainly driving the binary from the point of formation to a merger are strong ones. These include any encounter causing a significant ($\approx 10^{-3}$) narrowing of the semi-major axis.

### 3.1.2 Multiple random seeds

Figure 3.3 depicts four runs of the system from Askar et al. (2021) (see Table 2.1) evolving from log(a)/au$\approx$ 3.5 to -1. These are performed with different random seeds (motivated in Section 2.1.3) and are displayed along with merger times derived via Eq 1.1. For different random seeds, it took a different amount of time for the binary to evolve to a semi-major axis of $10^{-5}$ (see Table 3.1). They all exhibited the overall high but fluctuating eccentricity from Figure 3.1. This causes the runs to cross different astrophysical merger time contours at different points in their evolution. At some point in Figure 3.3, all seeds cross a merger time contour of at least 1 Myr. In a paper by Georgiev & Böker (2014), the youngest observed NSC was 1-2 Gyrs old. This would allow the binaries in Figure 3.3 plenty of time to merge within the lifetime of the NSC.

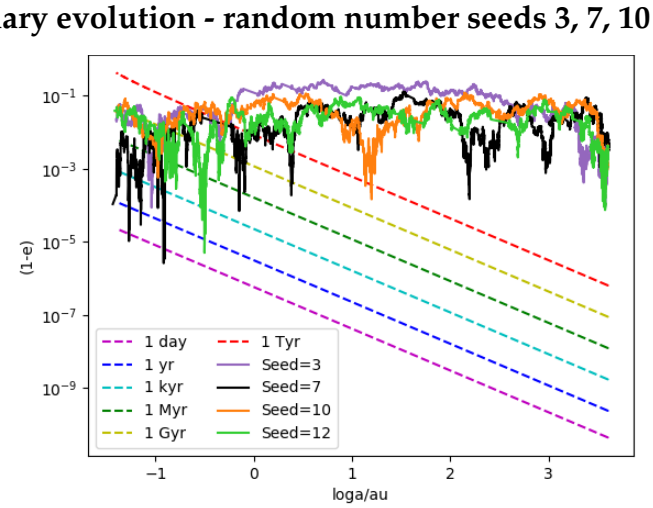


**Figure 3.3:** Same system (properties in Table 2.1) evaluated in accordance with Section 2.1.3 but with different random seeds. For seeds=3, 7, 10 and 12 it took $3.9{\cdot}10^5$, $3.8{\cdot}10^5$, $2.4{\cdot}10^5$ and $3.0{\cdot}10^5$ encounters respectivley to reach a semi-major axis of $4 \cdot 10^{-2}$. The diagonal lines are merger times derived from Eq 1.1. All runs manage to cross merger times smaller than the age of the Universe ($\approx 10^{10}$: Lattimer & Schramm 1976).

All runs share a strong hardening trend and managed to reach merger times below the Hubble time ($\approx 10^{10}$ yrs: Lattimer & Schramm 1976). This tells me there is efficient hardening and eccentricity pumping, i.e subsequent encounters at apocentre (see Section 1.1), under the relevant assumptions. These assumptions include the value of $C$ (Section 2.1.1), the initial setup (Table 2.1) and the distributions of $b$ (Section 2.1.1) and $v_\infty$ (Section 2.1.1).

### 3.1.3 Merger times

As presented in Chapter 1, a merger is most likely to occur when the merger time from Eq 1.1 is lower than the average time between encounters in Eq 1.2. However, a boundary of encounters was set in Section 2.1.1. This means that there will be weaker encounters not accounted for in the data presented in Figures 3.1 and 3.3. This should not affect the evolution of the binary (see Figure 3.2) but maybe a potential merger. However, it is obvious that the systems in Figures 3.1 and 3.3 reach short merger times and should merge within the time here simulated. So, instead of looking at when the encounter time surpasses the merger time, I chose to look at, what I call, the *total merger time*. This is the cumulative encounter times from Eq 1.2 at each point in time added to the instantaneous merger time. This is formalized

as

$$\tau_{merger,j} = \sum_{i=0}^{i=j-1} \Delta t_{enc,i} + \tau_{gr,j} \tag{3.1}$$

and is representative of the interplay between gravitational wave emission and encounters. So what Eq 3.1 gives me is the total time from the initial conditions to a fully merged binary, which in the optimal case is an SMBH seed. Eq 3.1 was used to extrapolate the total merger times of all four runs displayed in Figure 3.3. One of these runs is presented in Figure 3.4.

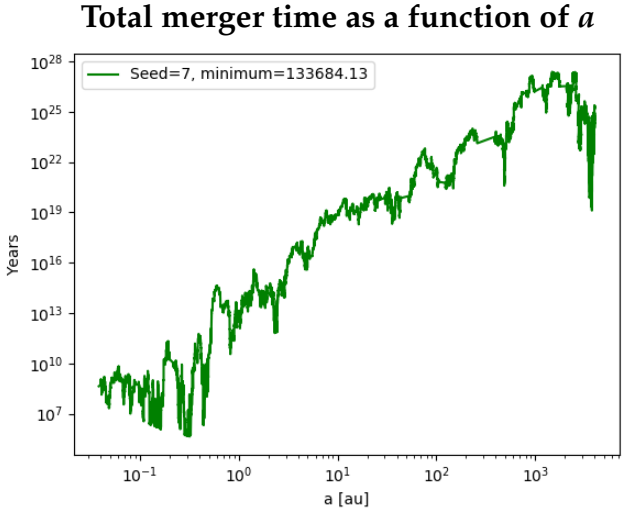


**Figure 3.4:** The total merger time at each instance in time is given by Eq 3.1. Its minimum value is the shortest time to go from initial conditions to being fully merged. It corresponds to the value of $a$ where it is most likely that the GW merger dominates the evolution and the binary merges. This plot used the data from Figure 3.1. Note that the binary starts at a=4000 au and decreases over time, meaning the plot should be interpreted from right to left.

Where the function has its lowest dip corresponds to the value of $a$ where GW merger starts to dominate the dynamic evolution of the system. This is where a merger is expected to occur. In other words, this is the value of $a$ the binary is expected to reach before merging via emission of GW. The value of Eq 3.1 at this $a$ is how long the full process takes from initial conditions to SMBH seed. The minimum values of Eq 3.1 when applied to the data from Figure 3.3 can be observed in Table 3.1 along with the full times of the respective simulations. The minimum values differed between the runs but not to such a degree that it could not be motivated by their stochastic nature.

**Table 3.1:** The minimum total merger times extrapolated via Eq 3.1 on the runs in Figure 3.3, in a similar way to what is displayed in Figure 3.4, along with the total simulated times.

| Random seed | Total merger time [Myrs] | Total simulated time in Fig 3.3 [Myrs] |
|---|---|---|
| 3 | 3.063 | 14.357 |
| 7 | 0.134 | 15.814 |
| 10 | 3.009 | 12.291 |
| 12 | 0.449 | 14.924 |

## 3.2 Comparison to Askar et al. (2021)

### 3.2.1 Toy model

This project aims to recreate and improve the accuracy within the Toy model presented by Askar et al. (2021). The results from the Toy model are displayed in Figure 3.5 along with the run from Figure 3.1 and the N-body run by Askar et al. (2021). It can there be observed that especially the Toy model exhibits some prominent differences from characteristics seen in Figure 3.1.

In the Toy model and the Seed=7-run in Figure 3.1, an eccentricity pumping is observed. However, this is a more prominent feature in the Toy model than in Figure 3.1. What the Toy model does not manage to achieve is a small enough semi-major axis. The given motivation was the assumption that each encounter only affected one IMBH and not the binary as a whole (Askar et al. 2021). In this thesis, all encounters are assumed to affect the whole binary at once which explains the lack of extreme eccentricity pumping but might be what allows for a more narrow semi-major axis.

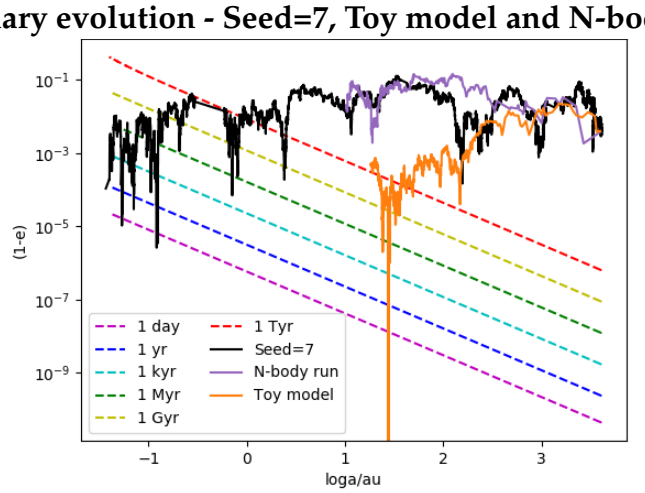


**Figure 3.5:** The data from the Toy model and N-body run by Askar et al. (2021) along with the run from Figure 3.1. It is visible how the Toy model has the most prominent eccentricity pumping whilst the seed=7-run has the most narrowing of the semi-major axis.

The largest divergence in Figure 3.5 is that of the Toy model at log(a) around 1 to 2. Here the eccentricity pumping goes to an extreme and it is clear that the Toy model should have a shorter merger time than the other runs. To further clarify to what degree the Toy model aligns or diverges from the runs in Figure 3.3 and 3.5, Figure 3.6 was produced. Figure 3.6 is a normalized plot illustrating the number density of eccentricity values in the semi-major axis range log(a)=(1,2).

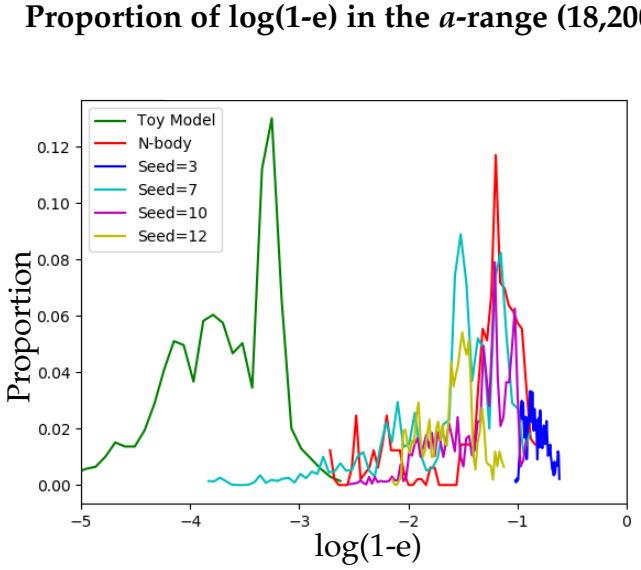


**Figure 3.6:** Normalised plot of the density as a function of (1-e) over the last relevant range of $a$ for the N-body run and Toy model.

Here, it is clear that the Toy model diverges from all the other runs. The runs produced in my simulations span a wide range but seem to be centered at the far right whereas the Toy model does not overlap with either the majority of the seeds or the N-body run. This tells me that it acts very differently from all of the others. Not being able to identify identical errors in my own and the N-body code, I feel urged to discourage the Toy model data. It seems as if the assumptions embedded in it exclude necessary physics and leads it to display a misleading representation of an IMBH binary evolution via low-mass impactors.

### 3.2.2 N-body run

That the N-body run in Figure 3.5 exhibits less binary hardening than the Toy model is something that Askar et al. (2021) mentions as being a result of the amount of movement the IMBHs are allowed to have during their evolution. In practice, this means that there are parts of the energy in the N-body run's encounters that go toward the binary recoiling. In the Toy model and in my simulations, on the other hand, all of the exchanged energy is transformed into kinetic energy of the third body. However, it can be observed that the binary here investigated, seen as Seed=7 in Figure 3.5, hardens without difficulty. Therefore, the difference in hardening, however non-prominent, between the N-body run and the Toy model would be caused by some other difference rather than the IMBHs freedom of movement.

It is also possible that the difference in hardening between the here performed runs and those done by Askar et al. (2021) is due to non-aligning stopping conditions. The runs in Figure 3.3 ran until a semi-major axis of order $10^{-5}$ had been reached (see Table 3.1) whereas the N-body run ran for 914 Myrs. In Section 1.1 it is stated how my model assumes there always being stars with orbits close enough to interact with the IMBH binary. This was not the case in the N-body run which leads to differences in, for example, simulated time.

## 3.3 Set parameters

### 3.3.1 Mass ratio

Initially, a reconstruction of the toy model in the paper by Askar et al. (2021) was attempted. This entailed masses of $10^3$, $10^2$ and 1 $M_\odot$. Following the reconstruction, the mass ratio between the components and the third body was investigated. This was done via plotting of $e$ over the change in $a$ and detecting where there was hardening (see Section 1.1), widening, no interaction or destruction. Here, I am not shining a light on specific values but choosing to focus on orders of magnitude. It should also be noted that a re-assessment of the proportionality constant $C$, relating $r_{peri}$ to the size and shape of the orbit, was not done. If the findings here presented

are to be further elaborated on, such a re-assessment should be done since Eq 2.2 tells us that $C$ has a mass dependence.

Seen in Figure 3.7a is the evolution of the system where the third body's mass is 10 $M_\odot$. Here, the binary shrinks faster than in Figure 3.1 with the desired eccentricity pumping, needed for reaching a shorter merger time, not being observed. This tells me that the binary initially is effectively softer and hence is less affected by strong encounters (Heggie 1975b). This explains why it looks dissimilar to Figure 3.1 where the opposite is the case.

Less extreme values of $e$ can be observed for the lower values of the semi-major axis in Figure 3.7a which translates to hardening being a more prominent feature of the evolution than eccentricity pumping. This results in fewer crossings with the merger time contours and causes the system to have a longer final merger time than the evolution displayed in Figure 3.1. If this is always the case is something that can be neither confirmed or rejected until more reconstructions have been completed.

The evolution of a system with a third mass on the order of 0.1 $M_\odot$, is seen in Figure 3.7b. The change were too small to be deemed relevant for a realistic timeline of a merger. The ratio generating the most noticeable change in parameters was with a third body with the mass of 1 $M_\odot$ as illustrated in Figure 3.1.

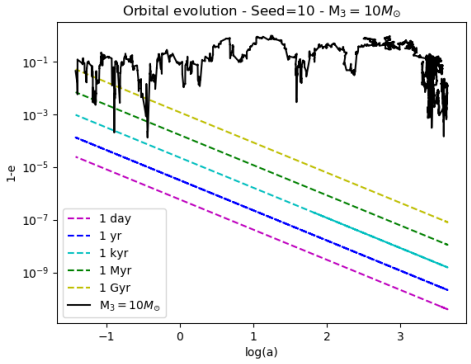


**(a)** One minus eccentricity over semi-major axis for an evolution with an impacting mass of 10 $M_\odot$. Far fewer encounters than in Figure 3.3, around 50 thousand, got the binary to the desired semi-major axis. However, the eccentricity pumping is not sufficient for the merger time to be shorter than the runs with a third mass of 1 $M_\odot$.

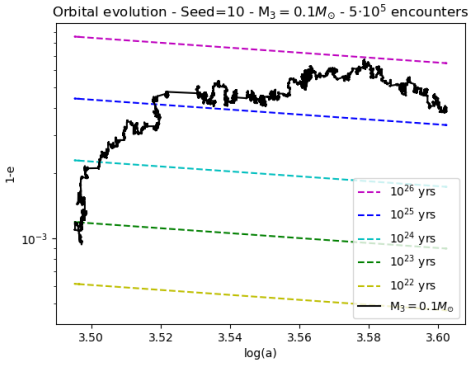


**(b)** With an impacting mass of 0.1 $M_\odot$ the system evolves slower. During 500 thousand encounters, the astrophysical merger time stays longer than the Hubble time ($\approx 10^{10}$: Lattimer & Schramm 1976). Therefore, the timescale of merging an IMBH binary via only 0.1 $M_\odot$ impactors and GWs could be unreasonably long.

**Figure 3.7:** Plots of one minus eccentricity over semi-major axis illustrates the evolution of my system but with altered third mass. Either the eccentricity does not evolve as far or the evolution is too slow. It can be concluded that out of the three cases, the mass ratio ($10^3$, $10^2$, 1) $M_\odot$ was the most efficient.

### 3.3.2 Initial eccentricity

All runs up until this point were executed with an initial eccentricity of 0.996 as given by Askar et al. (2021) and displayed in Table 2.1. But to see the effect on the system, Figure 3.8 was executed with an initial eccentricity of 0.5. This means that the binary starts off more circular than when the initial eccentricity was 0.996.

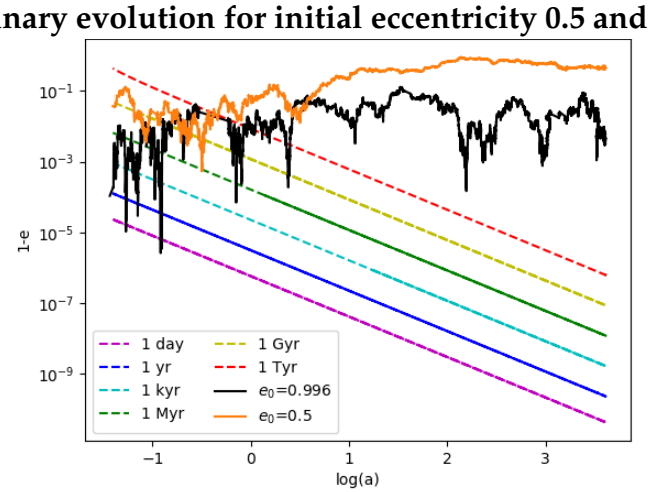


**Figure 3.8:** The evolution of the same massed system with an initial eccentricity of 0.5 and 0.996 along with merger time from Eq 1.1. The $e_0 = 0.5$ binary experiences $1.8{\cdot}10^5$ encounters and the $e_0 = 0.996$ binary $3.8{\cdot}10^5$ encounters. As the evolution goes from right to left, the system with an initial eccentricity of 0.5 fluctuates less and does not cross as low merger times as its e=0.996 counterpart. The runs become similar at about log(a)=0.5.

What can be seen is that there are fewer eccentricity fluctuations along with a less prominent eccentricity pumping. These features combine into a system that takes longer to reach the same merger time contours as the Seed=7-run and has an overall less eccentric shape. However, similar hardening to that in Figure 3.1 is still observable and the runs do eventually become similar, or consistent, at around log(a)≈0.5. The runs becoming similar means that from this point on, the conditions of the runs are indistinguishable. The values of the orbits are not connected to their initial conditions but only a result of the encounters.

The hardening, but not the eccentricity pumping, being comparable to that of the run in Figure 3.1 could indicate that hardening is generally a more dominant feature of my simulations than eccentricity pumping, resulting in the system always reaching similar merger times eventually. By Eq 1.1 the most likely total merger time of the $e_0$=0.5 run in Figure 3.8 was 1.207 Myrs. This is within the range displayed in Table 3.1 which could indicate that the initial eccentricity is not what dictates the final merger time. More runs would have to be conducted for this to be certain.

It could be that the high values of $e$ seen throughout the runs in Figure 3.3 are a consequence of the runs' high initial eccentricity and not only an outcome dictated by an always present eccentricity pumping. Another possibility is that the system illustrated in Figure 3.8 would eventually reach similar high values of eccentricity to Figure 3.3 but that the simulated time is too short.

# Chapter 4

# Discussion

So, it turns out that the mechanism described by Askar et al. (2021) is observable in these simulations as well. There is a consecutive hardening and a tendency towards high values of $e$ that combined leaves the binary to have a significantly reduced astrophysical merger time. However, what is displayed in Figure 3.3 is qualitatively different from the Toy model in Figure 3.5. This is due to the differences in dynamic assumptions done during the two evolutions. When assuming the encounters only affect one body, as is the case in the Toy model, an excessive eccentricity pumping is observed. When accounting for more of the necessary physics, the evolution goes more towards the N-body run in Figure 3.5 but without prominent obstacles for hardening of the binary. This demonstrates and reinforces the theories regarding IMBH merger as a possible origin of SMBH seeds.

The encounters driving the evolution were established to be strong ones where the change in the semi-major axis and eccentricity is prominent. It was clear, when investigating mass ratios, that the reduced merger time is partly due to the choice of the impactor's mass.

## 4.1 The third body's constant mass

As mentioned in Section 2.1.1, all third body masses were assumed to be 1 $M_\odot$ when producing Figure 3.3. This assumption offered simplicity but should be re-evaluated when expanding the physical validity of the model. Such an expansion is by Heggie (1975b) stated to be trivial. The NSC contains stars of multiple masses (Genzel et al. 2010). The majority of the stars in the NSC are old, meaning they are older than 1 Gyr, and have masses of about 0.5-4 $M_\odot$ (Genzel et al. 2010). However, there is also the presence of younger stars. This leads to the initial mass function covering a range of masses from 0.1 to 120 $M_\odot$ (adapted from Bartko et al. (2010): Genzel et al. 2010).

Thereby, negligence of the third body's mass range reduces the reliability of the evolutions presented in this paper. Both the N-body run and the Toy model utilize a distribution of third masses. This flaw in my own model could be partly remedied by making a similar probability distribution for the third body's mass as was done for $b$ in Section 2.1.1. By Aarseth (1971) it was presented that including a mass distribution, rather than a constant mass, of the impacting body would speed up the evolution of the encountered binary. It is therefore assumed that the efficiency of the evolution would be effected if a revision were to be done.

Moreover, the stellar properties of the third body are not something to be taken as a non-questionable fact. As illustrated in Figure 3.7b, hardening is still present with a larger mass third body. Therefore, stellar-mass black holes in the NSC (Chen et al. 2023) should not be excluded as third-body candidates.

## 4.2 Narrowing the margins of encounters

Another constant parameter, given in Section 2.1.1, is the proportionality constant $C$. This was set to its maximum to allow for the biggest range of encounters possible. This was done as a precaution to ensure no dominant encounters were missed. But when looking at Figures 3.2a and 3.2b it is clear how upping the lower limit of encounters would not significantly alter the outcome of the evolution in Figure 3.1.

The value of $C$ can be translated into how wide encounters are allowed to be. So when doing the same evolution as in Figure 3.1 but with a larger value of $C$ it is not surprising that there are regions of less prominent fluctuations as well as the overall hardening and high eccentricity as previously seen. This is because the higher $C$ in Figure 4.1 should still have its evolution driven by the strong encounters, as was the case for Figure 3.1, but with a wider range of how impactful the encounters are. With it still being the case that all types of encounters are of similar likelihood to occur, and there being a wider spread of encounter types, the overall rate of all encounters, even very impactful ones, should be lowered.

Same as in Figure 3.8, the runs become consistent, or similar, at around log(a)=-0.5. Up until this point, the $C$=10 run exhibits lower values of $e$ than the $C$=6.12 run with the exception being at the start of its run. Here, at about log(a)=3.6, the eccentricity shoots to very high values. Whether this is a statistical fluke was not investigated here but should be if one is to further investigate the proportionality constant $C$. If it is not a statistical fluke, it indicates that weak encounters play a bigger part than was previously deduced from Figure 3.2.

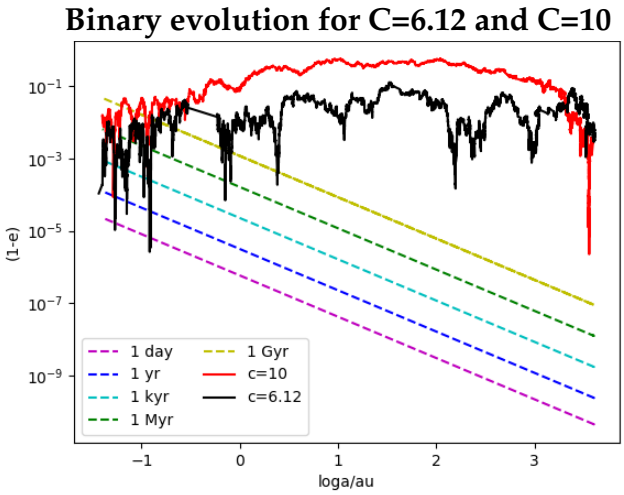


**Figure 4.1:** The same system evaluated in time with a proportionality constant $C$ of 6.12 or 10. A higher value of $C$ allows for wider, thereby weaker, encounters in alignment with Eq 2.2. This can be observed as the evolution being overall flatter.

The value of $C$ was set to its maximum, 6.12, over a range of $v_\infty$ (see Section 2.1.1). However, this was produced under the assumption that the initial eccentricity would be 0.5. After resetting the initial eccentricity to 0.996 it was not deemed a priority to re-evaluate the value of $C$. This reasoning had its base in there being little harm in allowing for too weak encounters. As presented in Section 3.3.2, the total merger time, when the initial eccentricity was 0.5, was within the range from Table 3.1 which further implies there being little harm in having $e_0 = 0.5$ instead of 0.996.

However, had a re-evaluation been done, it is believed that the value of $C$ would have been lower. This is based on the observations from Figures 3.2 and 2.2 where it is clear that large changes in $a$ are dominant in the evolution and are connected to low values of $b$. From Eq 2.2 it's clear that low values of $b$ would be connected to low values of $C$. Through Eq 3.1 it was found that the $C$=10 run in Figure 4.1 had a total merger time of about 3.991 Myrs. This hints towards the overall eccentricity pumping being marginally faster for a lower value of $C$ so a re-evaluation of $C$ should have increased the efficiency of the calculation.

## 4.3 Impact parameter $b$

From Eq 2.1 it is clear that the hardening of a binary is accompanied by narrower passes by encountering stars. This affects $b_{\max}$ through Eq 2.2. It is therefore necessary that the maximum impact parameter $b_{\max}$ evolves as the binary hardens. Neglecting this and keeping $b$ fixed (as discussed in Section 3.2.1) or non-elaborated on the shape $b_{\max}$=Ca(1+e) leads to a significant lowering of $e$ and does not result in

a merger time of reasonable order. Early on in the project, the latter was the case.

All plots presented in Chapter 3 were produced with Eq 2.2 and should therefore not lack credibility in their description of the discussed phenomenon. However, the limit of relevant encounters (Figure 2.2) and the value of $C$ were determined with the previous, faulty, version of $b_{max}$. The fact that no specific value was derived from Figure 2.2, but rather an order of magnitude, should partly compensate for this. Regarding the setting of $C$, where a value was extracted in part based on the value of $b_{max}$, it is thought that the only consequence was a too-inclusive model. This is further elaborated on in Section 4.2.

## 4.4 Point masses or not

When evaluating the validity of the here presented model, it should not be overlooked that all bodies, at all times, are assumed to behave as point masses. This means that all forms of tidal disruption are neglected. Were it instead considered, it is possible that the efficiency of the merger process would be different. The tidal disruption radius, the radius within which the black hole tidally disrupts other bodies, is given by Gezari (2021) to be

$$R_T = R_\star \left( n^2 \frac{M_{BH}}{M_\star} \right)^{1/3} \tag{4.1}$$

which here becomes about $r_{peri}$=0.05 au. This corresponds to rather strong encounters when the binary's semi-major axis is very narrow. These encounters could potentially carry away angular momentum and speed up the hardening via Eq 2.5 or do the opposite. Which one is the case, should be explored if the model is to be expanded with the inclusion of tidal disruption events. Gas accretion could contribute to a growth of the IMBHs (Askar et al. 2021) which would then affect the mass in Eq 4.1 and expand the tidal disruption radius. It could also, similarly to TDEs, extract angular momentum and speed up the evolution that way.

# Chapter 5

# Conclusions

Through N-body simulations, using the TSUNAMI code, the evolution of an IMBH binary encountering low-mass stars in an NSC was investigated. As suggested by Askar et al. (2021), I found that encounters enabled the IMBH binary to harden in accordance to Heggie (1975a) and its eccentricity to stay very high. It was found that the evolution was dominated by strong encounters when the impacting mass was about 0.1% of the largest mass in the system. The simulations stochastic nature made it hard to draw certain conclusions but all reached merger times between 0.1 and 3.1 Myr. According to the NSC ages found by Georgiev & Böker (2014), these merger times are sufficiently short for the binary to merge within the lifetime of the NSC. This reinforces the hypothesis of IMBH mergers occurring and being a possible origin of SMBH seeds.

It was observed that the Toy model presented by Askar et al. (2021) had an eccentricity pumping much greater than any of my simulations. When analyzing the assumptions it entailed and comparing its evolution to that in the N-body run and here performed simulations, it was concluded that it did not contain all the necessary physics to fully represent the evolution of the binary. One such assumption was that each encounter only affected one constituent of the binary. That was not the case in my simulations. However, I assumed the third mass to be constant and there to always be close enough stars to interact, something Askar et al. (2021) did not do. Regardless of this, my results were rather similar to that of the N-body simulation also presented by Askar et al. (2021).

It was found that it took the system longer to reach the desired merger time if the mass of the third body was reduced. It was suggested that a lowering of the initial eccentricity did not have much impact on the final merger time but this was merely speculative. Similarly, the width of encounters seemed to affect the evolution of the binary but additional simulations have to be carried out to ensure to what extent.

The uniqueness of each encounter brought physical reliability to the simulations where the velocity, impact parameter, and encounter times were dynamically motivated rather than set to a constant value. To further elaborate on the findings in this thesis, the assumption of point masses, the constant mass of the impactor, and the generous range of encounters should be re-assessed.

# Bibliography


Aarseth, S. J. 1971, , 14, 20

Aharon, D. & Perets, H. B. 2015, ApJ, 799, 185

Amaro-Seoane, P. & Freitag, M. 2006, ApJ, 653, L53

Antonini, F., Capuzzo-Dolcetta, R., Mastrobuono-Battisti, A., & Merritt, D. 2012, ApJ, 750, 111

Askar, A., Davies, M. B., & Church, R. P. 2021, MNRAS, 502, 2682

Bartko, H., Martins, F., Trippe, S., et al. 2010, ApJ, 708, 834

Begelman, M. C., Blandford, R. D., & Rees, M. J. 1980, Nature, 287, 307

Chen, Z., Do, T., Ghez, A. M., et al. 2023, ApJ, 944, 79

Dokuchaev, V. I. & Ozernoi, L. M. 1981, Soviet Astronomy Letters, 7, 52

Ebisuzaki, T., Makino, J., Tsuru, T. G., et al. 2001, ApJ, 562, L19

Freitag, M., Gürkan, M. A., & Rasio, F. A. 2006, MNRAS, 368, 141

Fujii, M., Iwasawa, M., Funato, Y., & Makino, J. 2009, ApJ, 695, 1421

Genzel, R., Eisenhauer, F., & Gillessen, S. 2010, Reviews of Modern Physics, 82, 3121

Georgiev, I. Y. & Böker, T. 2014, MNRAS, 441, 3570

Gezari, S. 2021

Greene, J. E., Strader, J., & Ho, L. C. 2020, ARA&A, 58, 257

Gürkan, M. A., Freitag, M., & Rasio, F. A. 2004, ApJ, 604, 632

Heggie, D. C. 1975a, MNRAS, 173, 729

Heggie, D. C. 1975b, in Dynamics of the Solar Systems, ed. A. Hayli, Vol. 69, 73

Hénon, M. 1972a, in Astrophysics and Space Science Library, Vol. 31, IAU Colloq. 10: Gravitational N-Body Problem, ed. M. Lecar, 44

Hénon, M. 1972b, in Astrophysics and Space Science Library, Vol. 31, IAU Colloq. 10: Gravitational N-Body Problem, ed. M. Lecar, 406

Kaczmarczyk, K. & Miałkowska, K. 2022, Procedia Computer Science, 207, 1901

Larson, R. B. 1970a, MNRAS, 147, 323

Larson, R. B. 1970b, MNRAS, 150, 93

Lattimer, J. M. & Schramm, D. N. 1976, ApJ, 210, 549

Leigh, N. W. C., Böker, T., Maccarone, T. J., & Perets, H. B. 2013, MNRAS, 429, 2997

Loose, H. H., Kruegel, E., & Tutukov, A. 1982, A&A, 105, 342

Madau, P. & Rees, M. J. 2001, ApJ, 551, L27

Magorrian, J. & Tremaine, S. 1999, MNRAS, 309, 447

Mastrobuono-Battisti, A., Perets, H. B., & Loeb, A. 2014, ApJ, 796, 40

Mikkola, S. & Tanikawa, K. 1999a, MNRAS, 310, 745

Mikkola, S. & Tanikawa, K. 1999b, Celestial Mechanics and Dynamical Astronomy, 74, 287

Neumayer, N., Seth, A., & Böker, T. 2020, , 28, 4

Peters, P. C. 1964, Physical Review, 136, 1224

Portegies Zwart, S. F., Baumgardt, H., Hut, P., Makino, J., & McMillan, S. L. W. 2004, Nature, 428, 724

Portegies Zwart, S. F., Baumgardt, H., McMillan, S. L. W., et al. 2006, ApJ, 641, 319

Ryden, B. & Peterson, B. M. 2021a, in Foundations of astrophysics 4th edition (Cambridge University Press), 111–146

Ryden, B. & Peterson, B. M. 2021b, in Foundations of astrophysics 4th edition (Cambridge University Press), 61–83

Spitzer, Lyman, J. & Hart, M. H. 1971a, ApJ, 164, 399

Spitzer, Lyman, J. & Hart, M. H. 1971b, ApJ, 166, 483

Trani, A. A. & Spera, M. 2020, Proceedings of the International Astronomical Union, 16, 404

Tremaine, S. D., Ostriker, J. P., & Spitzer, L., J. 1975, ApJ, 196, 407

Tsatsi, A., Mastrobuono-Battisti, A., van de Ven, G., et al. 2017, MNRAS, 464, 3720

Valtonen, M. J. & Karttunen, H. 2006, in The three-body problem. (Cambridge University Press)

Volonteri, M. 2010, , 18, 279

Wirth, H. & Bekki, K. 2020, MNRAS, 496, 921

# Acknowledgements

I would like to thank Ross Church for his patient and enthusiastic guidance throughout this project. My parents Roland and Lalla Thord, as well as my brothers Ludvig and Rasmus Thord, are my biggest joys and comforts with their tireless listening to my theories and endless support in my undertakings. You taught me to reach for the stars. For all the support, I wish to thank Helena Cronstedt, Nikolaj Skog Pirinen, Carl Pettersson and my beloved Allan Stenberg. I would also like to direct an homage to my trustworthy cheerleaders: Ebba Larsson, Elsa Ängmo von Borstel, Max Persson Kristiansson, Stinalisa Andersson, Henry Lockett and Adrian Eylers. Lastly, I will always be grateful to Mats Johannesson, Sara Dahl and Uffe Holmström for being my safe spaces and inspiration. This work is dedicated to my grandmother Maj Bohman, a never-fading light in the darkness.